



Reynolds Number Dependence of the Structure Functions in Homogeneous Turbulence

John Kaminsky¹ · Björn Birnir^{1,3} · Gregory P. Bewley² · Michael Sinhuber⁴

Received: 16 October 2018 / Accepted: 3 December 2019 / Published online: 1 January 2020
© Springer Science+Business Media, LLC, part of Springer Nature 2020

Abstract

We compare the predictions of stochastic closure theory (SCT) (Birnir in *J Nonlinear Sci* 23:657–688, 2013a. <https://doi.org/10.1007/s00332-012-9164-z>) with experimental measurements of homogeneous turbulence made in the variable density turbulence tunnel (Bodenschatz et al. in *Rev Sci Instrum* 85(9):093908, 2014) at the Max Planck Institute for Dynamics and Self-Organization in Göttingen. While the general form of SCT contains infinitely many free parameters, the data permit us to reduce the number to seven, only three of which are active over the entire range of Taylor–Reynolds numbers. Of these three, one parameter characterizes the variance of the mean-field noise in SCT and another characterizes the rate in the large deviations of the mean. The third parameter is the decay exponent of the Fourier variables in the Fourier expansion of the noise, which characterizes the smoothness of the turbulent velocity. SCT compares favorably with velocity structure functions measured in the experiment. We considered even-order structure functions ranging in order from two to eight as well as the third-order structure functions at five Taylor–Reynolds numbers (R_λ) between 110 and 1450. The comparisons highlight several advantages of the SCT, which include explicit predictions for the structure functions at any scale and for any Reynolds number. We observed that finite- R_λ corrections, for instance, are important even at the highest Reynolds numbers produced in the experiments. SCT gives us the correct basis function to express all the moments of the velocity differences in turbulence in Fourier space. These turn out to be powers of the sine function indexed by the wavenumbers. Here, the power of the sine function is the same as the order of the moment of the velocity differences (structure functions). The SCT produces the coefficients of the series and so determines the statistical quantities that characterize the small scales in turbulence. It also characterizes the random force acting on the fluid in the stochastic Navier–Stokes equation, as described in this paper.

Mathematics Subject Classification 76F05

Communicated by Charles R. Doering.

Extended author information available on the last page of the article

1 Introduction

Let us begin with a brief history of wind tunnel research and of the effort to describe the structure of turbulence statistically. In aeronautics, the design of airfoils and airplanes was a major challenge. The development of appropriate laboratory experiments facilitates progress to this day, including the invention of the wind tunnel. The first wind tunnel is credited to F. Wenham in Great Britain in 1871. The Wright brothers also constructed their own wind tunnel in 1901 (Baals and Corliss 1981), but it was Ludwig Prandtl who designed the first “modern” wind tunnel. This 1917 tunnel was actually his second design, his first design in 1909 being a closed-loop wind tunnel which, by his own admission, was “of a temporary nature” (Prandtl 1920). Nonetheless, his second, more permanent design would become the model for many subsequent wind tunnels (Anderson 1999). Prandtl’s student, Max Munk, went on to design the first wind tunnel that allowed adjustment of the density of the working fluid (Bodenschatz et al. 2014), and so for much higher Reynolds number flows in the tunnel. This tunnel was built at the Langley Research Center in Virginia in 1923. Most of the early research done with wind tunnels was devoted to the study of airfoils and airplane shapes and Mach number (Bodenschatz et al. 2014). One interesting feature of these tunnels was the ability to adjust Mach number and Reynolds number independently.

Wind tunnels are essential tools to study not only airfoils and model airplanes, but also to study statistically homogeneous and isotropic turbulence, see Taylor (1935). Such flows limit turbulence to its essential ingredients: inertia, pressure and friction, minimize the effects of the boundaries on the flow and do not exhibit a preferred orientation. It can be created by mechanically stirring a liquid or gas (Bodenschatz et al. 2014). A close approximation of such flows is realized in a wind tunnel when a uniform free-stream flow is disturbed by a mesh or a grid, see Comte-Bellot and Corrsin (1966) and Corrsin (1961).

Experiments to study turbulence were rare until the second half of the twentieth century. The 1940s featured experiments on grid turbulence in California (Millikan et al. 1948), while another series of experiments were performed at the Nuclear Research Lab in Jülich in the 1970s (Hunt et al. 1992). More recently, wind tunnels were built at the German Aerospace Center in Göttingen and at the Princeton Gas Dynamics Lab with similar goals. The experiments in this paper were performed in the facility at the Max Planck Institute for Dynamics and Self-Organization in Göttingen called the variable density turbulence tunnel (VDTT), which was completed in 2009 (Bodenschatz et al. 2014). It has achieved turbulent flow up to Taylor–Reynolds number 1600, which is the highest recorded for a passive grid experiment until that time, with higher Reynolds number since being recorded with an active grid (Sinhuber et al. 2015, 2017). Details about the VDTT can be found in Bodenschatz et al. (2014). One of the Prandtl’s original wind tunnels sits beside the VDTT in Göttingen, see Bodenschatz et al. (2014).

The mathematical theory of turbulence has its roots in the work of Kolmogorov. In 1941, Kolmogorov published his celebrated four-fifths law and postulated, together with Obukhov, that the structure functions of turbulence of n th order, S_p , should scale

with the lag variable, r , so that

$$S_p(x, y, t) = E(|u(x, t) - u(y, t)|^p) = C_p r^{p/3},$$

where p is the order of the structure function and $r = |x - y|$, where x and y are the positions in space. Lev Landau criticized the theory for neither taking into account the organization of the flow on large scales nor the influence of intermittency, which is the development of long tails in the velocity difference distributions at large Reynolds numbers (Birnik 2013a). In 1962, Kolmogorov and Obukhov revised their theory to address these criticisms. They introduced a correction to the exponent, such that

$$S_p(x, y, t) = C_p \epsilon^{\frac{p}{3}} r^{\frac{p}{3} + \tau_p} = C'_p r^{\frac{p}{3} + \tau_p} = C'_p r^{\zeta_p},$$

where ϵ is the dissipation rate and $\zeta_p = \frac{p}{3} + \tau_p$, and τ_p is a correction that needs to be determined. A prediction for the correction was found by She and Leveque (1994):

$$\tau_p = -\frac{2p}{9} + 2 \left(1 - \left(\frac{2}{3} \right)^{\frac{p}{3}} \right), \quad (1)$$

see She and Leveque (1994). In Birnik (2013a), the log-Poisson processes of Dubrulle (1994) and She and Waymire (1995), responsible for the intermittency corrections, were derived from the stochastic Navier–Stokes equation.

Kolmogorov and Obukhov considered the velocity in turbulent flow to be a stochastic process, and their hypotheses include that the 2-point probability distribution function (PDF) of turbulence does not depend on x or y individually but only on r , ν and ϵ , where r is the lag variable, ν is the kinematic viscosity, and ϵ is the kinetic energy dissipation rate of the turbulence per unit mass (Pope 2000). Moreover, when $r \gg \eta$, where η is the Kolmogorov (or dissipation) scale, the PDF depends on ϵ and r alone, and not on ν . Since the 2-point PDF determines the structure functions described above, the same statements that apply to the PDFs apply also to the structure functions.

If the turbulent velocity is a stochastic process, it must satisfy a stochastic Navier–Stokes equation. Such an equation was formulated by Landau and Lifschitz in their Fluid Dynamics book (Landau and Lifshits 1959). They considered the noise in the stochastic Navier–Stokes equation to be the source of fluctuations in the velocity, which cannot be ignored in turbulence. They argued that it should be white both in time and space, but this assumption cannot be true since the Navier–Stokes equation driven by noise that is white in space produces velocities that are not continuous (Walsh 1984), and this is not observed in nature. Birnik (2013a) argued that the noise has enough smoothness in space that the dissipation rate, ϵ , is finite, and that the noise is of a generic nature that includes an additive term corresponding to a mean-field noise and another additive term corresponding to the large deviations of the mean field. He also added a multiplicative noise term, modeling jumps in the gradient for the flow velocity, and showed that this term produced the log-Poisson process of Dubrulle, She and Waymire and their intermittency corrections τ_p . These assumptions are the basis

of the stochastic closure theory (SCT) (Birniir 2013b) and are elaborated in the next section.

2 The Assumptions of SCT and Its Predictions

The following assumptions produce the stochastic Navier–Stokes equation (7) given in the next section. The detailed arguments leading to the form of the noise are given in Birniir (2013a, b). They follow the spirit of the argument in Landau and Lifshits (1959). We also list the predictions of the theory, which include a quantitative prediction of the She–Leveque intermittency corrections to the Kolmogorov–Obukhov ’62 theory of turbulence.

SCT Assumptions:

1. The small scale flow in fully developed turbulence satisfies a stochastic Navier–Stokes (SNS) equation.
2. The noise in the SNS consists of both an additive and a multiplicative term.
3. The additive noise is in part a general mean-field noise that is sufficiently smooth in space for the dissipation rate:

$$\epsilon = \nu \int_{\Omega} |\nabla u|^2 dx < \infty,$$

to be finite. In addition to this “infinite-dimensional Brownian” mean-field noise, there is a deterministic additive part that captures large deviations in the mean field.

4. The multiplicative noise models jumps in the velocity gradient, ∇u . This term is then multiplied by the velocity u . It is the noise associated with the inertial term in the Navier–Stokes equations.
5. The most singular (having least spatial smoothness) structures in (3-d) turbulence are one-dimensional vortex lines.

SCT Predictions:

1. The structure functions of turbulence at finite Reynolds numbers are given by formulas that explicitly incorporate the Reynolds number dependence of the structure functions.
2. The N-point probability density function exists and can be computed. In the two-point case, it is determined by the Kolmogorov–Hopf functional differential equation (Birniir 2013b) and has an explicit formula (Birniir 2016).
3. There exists an invariant measure on the phase space of the stochastic Navier–Stokes equation (Birniir 2013b, 2016). This measure has an explicit formula (Birniir 2016), and the stochastic Navier–Stokes flow is ergodic with respect to this measure.
4. The PDF for the velocity distribution in turbulence is a generalized hyperbolic distribution (Barndorff-Nilsen 1977) convolved with the Poisson distribution of the log-Poisson processes of Birniir 2016. For large values of the lag variable and

for the fluid velocities themselves, these distributions become (skewed and flat) Gaussians.

The most important SCT prediction for this paper is (1), the explicit formulae for the structure functions with given Reynolds number dependencies. We use these formulas to fit the data measured in the VDTT, and this is the subject of the paper. A disadvantage of equation is that the noise has infinitely many undetermined coefficients c_k , d_k and h_k . The last coefficients are a consequence of assumption 3 above. The vorticity lines are one dimensional, and this implies that all the coefficients, h_k , are fixed (Birnir 2013b). However, we are still left with infinitely many coefficients c_k and d_k . What we find through comparison with the experimental data is that, after fitting the characteristics of the VDTT and non-isotropy, we can reduce the number of coefficients to only three. When the mean flow is given, we are left with one parameter that characterizes the infinite-dimensional Brownian, another parameter characterizing large deviations from the mean, and one exponent characterizing spatial smoothness. We find, as expected, that the mean flow and the three parameters depend on the Taylor–Reynolds number. They do not, however, depend on the order of the structure function. The upshot is a much improved stochastic closure model (26) with only three parameters characterizing the noise.

One can say that the SCT produces the correct basis, with basis functions that are functions of the lag variable indexed by the wavenumber, to represent all the statistical quantities of the velocity differences. This is a big improvement over previous theoretical result that only produces one or finitely many statistical quantities measurable in experiments.

3 The Stochastic Closure Model

In this section, we give a short derivation of the SCT model. We first explain how the form of the turbulent noise forcing, in the Navier–Stokes equation, is derived and then use some techniques from probability theory to transform the resulting stochastic Navier–Stokes equation, for the small-scale velocity, to an integral equation. The integral equation will be used in the next section to compute a sharp lower estimate for the structure functions. The reader is directed to Birnir (2013b) for more details.

The flow in the wind tunnel is governed by the Navier–Stokes equation:

$$\begin{aligned} u_t + (u \cdot \nabla)u &= \nu \Delta u - \nabla p, \\ \operatorname{div} u &= 0, \\ u(x, 0) &= u_0(x), \end{aligned} \quad (2)$$

where $u(x)$ is the fluid velocity, $x \in \mathbb{R}^3$, p is the pressure, and ν is the viscosity. We also impose periodic boundary conditions upon the flow. The second line in (2) is the incompressibility condition. Using this equation, we can eliminate the pressure to get

$$u_t + u \cdot \nabla u = \nu \Delta u + \nabla(\Delta^{-1}[\operatorname{Trace}(\nabla u)^2]). \quad (3)$$

This equation defines the evolution of the velocity of the fluid in time. We will impose periodic boundary conditions on the small scales below.

Following the classical Reynolds decomposition (Reynolds 1885), we decompose the velocity into mean flow U and the fluctuations u . Then, the velocity is written as $U + u$, where U describes the mean or large-scale flow and u describes the velocity fluctuations. These two terms describe the large scales and small scales of the flow, respectively. If we also decompose the pressure into mean pressure P and the fluctuations p , then the equation for the large-scale flow can be written as

$$U_t + U \cdot \nabla U = \nu \Delta U - \nabla P - \nabla \cdot (\overline{u \otimes u}), \quad (4)$$

where in coordinates

$$\nabla \cdot (\overline{u \otimes u}) = \frac{\partial \overline{u_i u_j}}{\partial x_j},$$

that is ∇ is dotted with the rows of $\overline{u_i u_j}$, and $R_{ij} = \overline{u \otimes u}$ is the Reynolds stress, see Bernard and Wallace (2002). The Reynolds stress has the interpretation of a turbulent momentum flux, and the last term in (4) is also known as the eddy viscosity. It describes how the small scales influence the large scales. In addition, from linearity, we get divergence free conditions for U and u

$$\nabla \cdot U = 0, \quad \nabla \cdot u = 0.$$

Together, (4) and the divergence free condition on U give the Reynolds-averaged Navier–Stokes (RANS) that forms the basis for most contemporary simulations of turbulent flow. The large-scale equation (4) is satisfied by the mean flow $U = \text{constant}$ in the measurement region of the VDTT. Thus, in our case, (4) reduces to the pressure gradient balancing the eddy viscosity.

The notation $\overline{u \otimes u} = E(u \otimes u)$ denotes the expectation that is assumed to be the same as an ensemble average $\overline{u \otimes u} = \langle u \otimes u \rangle$. Thus, when we discuss the mean large-scale flow \bar{U} and the mean small-scale (fluctuation) flow \bar{u} below, we mean the expectation or ensemble average of these quantities.

Finding a constitutive law for the Reynolds stress $\overline{u \otimes u}$ is the famous closure problem in turbulence, and we will solve that by writing down a stochastic equation for the small-scale velocity u . This was first done by Landau and Lifshits (1959).

The consequence of the SCT hypothesis is that the fluctuating velocity u in turbulence is a stochastic process that is determined by a stochastic partial differential equation (SPDE). It will be the Navier–Stokes equation for the fluctuations driven by noise, see below. This is the point of view taken by Kolmogorov (1941a, b, 1962), but the question we have to answer is: What is the form of the noise? There is a wide array of the literature on this question, trying to trace the form of the noise back to the fluid instabilities, but these attempts have proven to be unsuccessful. Any memory of the fluid instabilities is quickly forgotten in fully developed turbulence, and the noise seems to be of a general form. Thus, it makes sense to try to put generic noise into the Navier–Stokes equations and see how the Navier–Stokes evolution colors generic

noise. Below we will answer what generic noise in the Navier–Stokes equation must look like, see Birnir (2013b) for more details.

For fully developed turbulence, we close the model with a stochastic forcing term to account for the small scales in (2) and (3). This noise term models the dissipation in the flow. We impose periodic boundary conditions and then discretize on the torus. Let p_k denote the dissipation process in the j th box. We assume these dissipation processes in the flow are weakly coupled and have mean m . Thus, the average is given by

$$M_n = \frac{1}{n} \sum_{j=1}^n p_j.$$

We now make use of the central limit theorem, which implies M_n will converge to a Gaussian distribution with mean zero and variance one. For the statement and proof of the central limit theorem, see page 194 in Grimmett and Stirzaker (2001). Then, define

$$x_t^n = \frac{S_{[tn]} - nm}{\sqrt{n}\sigma},$$

where $S_n = \sum_{j=1}^n p_j$ and $[tn]$ denotes the integer value. We now apply the functional central limit theorem, as given by Theorem 8.1 in Bhattacharya and Waymire (1990), and so the processes x_t^n must converge in distribution to a Brownian motion b_t as $n \rightarrow \infty$. This must occur in the direction of any Fourier component and so we get

$$\bar{D} = \sum_{k \neq 0} c_k^{\frac{1}{2}} db_t^k e_k(x),$$

where $e_k(x) = e^{2\pi i k x}$ are the distinct Fourier components complete with its own Brownian motion b_t^k , and $c_k^{\frac{1}{2}}$ are the coefficients that converge sufficiently fast to ensure convergence of the entire series, see Birnir (2013b).

However, we also must measure the fluctuations in the dissipation which can be explained via the large deviation principle. To apply the large deviation principle, we need to describe the rate function associated with the process, which depends on whether the fluctuations are random. If they are, the fluctuations can be modeled by a Poisson process with rate λ , and furthermore, if there is bias in the fluctuations, then the deviations of M_n are bounded above by a constant determining the direction of the bias times the rate η . Cramer's theorem, see Birnir (2013b), then gives that the rate function is bounded by $\eta = \lambda$, and so the second additive noise term is

$$D' = \sum_{k \neq 0} d_k \eta_k dt e_k(x).$$

Here, $e_k(x)$ is defined as above, d_k is defined similarly to $c_k^{0.5}$, and η_k are the rates in the k th direction. We choose $\eta_k = |k|^{\frac{1}{3}}$ to line up with the scaling of the central limit theorem term. Thus, the large deviation principle gives the term

$$D' = \sum_{k \neq 0} d_k |k|^{\frac{1}{3}} dt e_k(x).$$

These two terms defined the additive noise forcing term. A more detailed description of these terms is given in Birnir (2013b).

A final forcing term comes from the multiplicative noise. This noise models jumps in the velocity gradient or vorticity concentrations, if we let N_t^k denote the number of velocity jumps associated with the k th wavenumber that have occurred by time t . This in turn implies that the differential

$$dN^k(t) = N^k(t + dt) - N^k(t)$$

denotes the number of jumps in the time interval $(t, t + dt]$. The multiplicative noise then has the form

$$J = \sum_{k \neq 0} \int_{\mathbb{R}} h_k(t, z) \bar{N}^k(dt, dz),$$

where h_k measures the size of the jump and \bar{N}^k is the compensated number of jumps. For more information on the multiplicative noise, see Birnir (2013b).

Thus, adding the terms \bar{D} , D' and, J multiplied by u , to the Navier–Stokes equation, we get a stochastic PDE describing the fully developed turbulent small-scale flow in the wind tunnel:

$$\begin{aligned} du + u \cdot \nabla u dt &= [v \Delta u + \nabla(\Delta^{-1}[\text{Trace}(\nabla u)^2]) - u \cdot \nabla U - U \cdot \nabla u] dt \\ &+ \sum_{k \neq 0} d_k |k|^{\frac{1}{3}} dt e_k(x) + \sum_{k \neq 0} c_k^{\frac{1}{2}} db_t^k e_k(x) \\ &+ u \sum_{k \neq 0} \int_{\mathbb{R}} h_k(t, z) \bar{N}^k(dt, dz). \end{aligned} \quad (5)$$

Notice that this equation cannot be reduced to the equation for homogeneous and isotropic turbulence, see Birnir (2013b), by the Galilean invariance of the Navier–Stokes equation. We drop the term $-u \cdot \nabla U$, in the equation above, since the mean flow U is constant for homogeneous turbulence and approximately constant in the wind tunnel, see Bodenschatz et al. (2014). The term $-U \cdot \nabla u$ can, however, not be dropped. Its effect will be computed in next section. An application of Girsanov's

theorem allows us to eliminate the $(-u \cdot \nabla u - U \cdot \nabla u)dt$ term at the cost of adding an exponential martingale:

$$M_t = \exp\left(-\int (U + u(B_s, s)) \cdot dB_s - \frac{1}{2} \int_0^t |U + u(B_s, s)|^2 ds\right),$$

where $B_t \in \mathbb{R}^3$ is an auxiliary Brownian motion, to each term in the Navier–Stokes equation:

$$\begin{aligned} du &= [v\Delta u + \nabla(\Delta^{-1}[\text{Trace}(\nabla u)^2])]M_t dt \\ &+ \sum_{k \neq 0} d_k |k|^{\frac{1}{3}} M_t dt e_k(x) + \sum_{k \neq 0} c_k^{\frac{1}{2}} M_t db_t^k e_k(x) \\ &+ u \sum_{k \neq 0} \int_{\mathbb{R}} h_k(t, z) \bar{N}^k M_t(dt, dz). \end{aligned} \tag{6}$$

For the statement and proof of Girsanov’s theorem, see pages 149–151 of Oksendal (1998). The martingale captures the effects of the large scales on the noise in the small-scale flow.

The Feynman–Kac formula allows us to eliminate the term

$$u \times \sum_{k \neq 0} \int_{\mathbb{R}} h_k(t, z) \bar{N}^k M_t(dt, dz)$$

at the cost of adding a log-Poisson process

$$\begin{aligned} e^{\int_s^t dq} &= \frac{1}{3} \left(\sum_{k \neq 0}^m \left\{ \int_0^t \int_{\mathbb{R}} \ln(1 + h_k) \bar{N}^k(ds, dz) \right. \right. \\ &\quad \left. \left. + \int_0^t \int_{\mathbb{R}} (\ln(1 + h_k) - h_k) m_k(ds, dz) \right\} \right) \end{aligned}$$

to each term in the Navier–Stokes equation. For the statement and proof of Feynman–Kac Formula, see pages 128–129 of Oksendal (1998). Thus, the new Navier–Stokes equation becomes

$$\begin{aligned} du &= [v\Delta u + \nabla(\Delta^{-1}[\text{Trace}(\nabla u)^2])]e^{\int_s^t dq} M_t dt \\ &+ \sum_{k \neq 0} d_k |k|^{\frac{1}{3}} e^{\int_s^t dq} M_t dt e_k(x) + \sum_{k \neq 0} c_k^{\frac{1}{2}} e^{\int_s^t dq} M_t db_t^k e_k(x) \end{aligned} \tag{7}$$

Finally, we use the definition of mild (or martingale) solutions of nonlinear stochastic partial differential equations (SPDE) in infinite-dimensional space:

Definition 3.1 Consider the initial value SPDE problem

$$du = (Au + F(t, u))dt + G(t, u)dB_t, \quad u(x, 0) = u_0.$$

A stochastic process $u(\omega, x, t)$ is a mild solution of this SPDE initial value problem (IVP) if

$$P \left(\int_0^t |u|_2^2(s)dt < \infty \right), \quad P \text{ a. s.}$$

and

$$u(t) = e^{At}u_0 + \int_0^t e^{A(t-s)}F(s, u(s))ds + \int_0^t e^{A(t-s)}G(s, u(s))dB_s, \quad P \text{ a. s.},$$

where P is the probability measure in the associated probability space (Ω, \mathcal{F}, P) .

For more information, see page 182 in Da Prato and Zabczyk (2014). One can then state a theorem for the existence of unique mild local (in time) solutions, see page 186 in Da Prato and Zabczyk (2014). Now, this theorem does not apply directly here, as the multiplicative noise concerns jumps and not only Brownian motion. However, a slight alteration of the proof gives local existence of solutions. The mild solution of the stochastic Navier–Stokes equation, governing fully developed turbulence, is given by

$$\begin{aligned} u = & e^{K(t)} e^{\int_0^t dq} M_t u^0 + \sum_{k \neq 0} c_k^{\frac{1}{2}} \int_0^t e^{K(t-s)} e^{\int_s^t dq} M_{t-s} db_s^k e_k(x) \\ & + \sum_{k \neq 0} d_k \int_0^t e^{K(t-s)} e^{\int_s^t dq} M_{t-s} |k|^{\frac{1}{3}} dt e_k(x), \end{aligned} \quad (8)$$

where K is the operator

$$K = \nu \Delta + \nabla \Delta^{-1} \text{Trace}(\nabla u \nabla), \quad (9)$$

M_t is the above exponential martingale, $e_k(x) = e^{2\pi i k x}$ is a Fourier component complete with its own Brownian motion b_t^k , and the coefficients $c_k^{\frac{1}{2}}$ and d_k decay fast enough so that the series converges, see Birnir (2013b), Chapter 1. This is also the integral form of the stochastic Navier–Stokes equation (7). The integral equation (8) is equivalent to the stochastic Navier–Stokes initial value problem (7) for the small scales. It will be our main tool in computing the structure functions. The operator K above has a potential $\nabla \Delta^{-1} \text{Trace}(\nabla u \nabla)$ that depends on both x and t ; thus, it does not have eigenvalues and does not generate a semigroup. But K generates a flow, that we have denoted $e^{K(t)}$ above and if we replace it by its time average and apply the ergodicity of the stochastic Navier–Stokes evolution, see the SCT prediction number 3 above, then we get an operator where the time average of the potential is equal to

the expectation. This gives an operator $\tilde{K} = \nu\Delta + C\partial_x^{2/3}$, where by ergodicity C is a constant, see Birnir (2013b), with eigenvalues that we denote $\lambda_k, k \in \mathbb{N}$. This will greatly simplify the computation of the structure functions in the next section. Instead of estimates of the structure functions as in Birnir (2013a), we get equality in the formulas.

4 The Computation of the Structure Functions

In this section, we describe the calculation of the structure functions of turbulence, which will be compared with the experimental data. Using the stochastic Navier–Stokes integral equation (8) from previous section, we have that

$$\begin{aligned}
 u(x, t) - u(y, t) & \tag{10} \\
 &= \sum_{k \neq 0} \left[\left(c_k^{\frac{1}{2}} \int_0^t e^{K(t-s)} e^{\int_s^t dq} M_{t-s} db_s^k \right. \right. \\
 & \quad \left. \left. + d_k \int_0^t e^{K(t-s)} e^{\int_s^t dq} M_{t-s} |k|^{\frac{1}{3}} ds \right) (e_k(x) - e_k(y)) \right], \tag{11}
 \end{aligned}$$

where $u(x, t)$ and $u(y, t)$ are the flow velocities at two points x and y in the wind tunnel. This permits us to describe the computation of the structure functions:

$$S_p(x - y, t) = E (|u(x, t) - u(y, t)|^p).$$

First, we note that the expectation is actually a composition of three expectations: one for the Brownian motions in the Fourier series representation of the noise, denoted E_b , another for the log-Poisson process, denoted E_p , and the third E_B for the auxiliary Brownian motion in the martingale in the last section. The log-Poisson expectation acts upon the term

$$e^{\int_s^t dq} = \exp \left\{ \frac{\frac{2}{3} \ln |k| + N_t \ln \left(\frac{2}{3} \right)}{3} \right\} = \left(|k|^{\frac{2}{3}} \left(\frac{2}{3} \right)^{N_t} \right)^{\frac{1}{3}},$$

given by the Feynman–Kac formula, see Birnir (2013b). Then, we get that

$$E_p \left(\left[|k|^{\frac{2}{3}} \left(\frac{2}{3} \right)^{N_t} \right]^{\frac{p}{3}} \right) = |k|^{-\left(-\frac{2p}{9} + 2 \left(1 - \left(\frac{2}{3} \right)^{\frac{p}{3}} \right) \right)},$$

see Birnir (2013b). Notice the exponent above is the She–Leveque intermittency correction (1), denoted τ_p . Applying E_p also eliminates all terms $(e_k(x) - e_k(y))(e_j(x) - e_j(y))$ for $k \neq j$. Standard algebra and trigonometry gives

$$e_k(x) - e_k(y) = 2e^{\pi i k(x+y)} \sin(\pi k \cdot (x - y)).$$

Thus, we get that

$$E(|u(x, t) - u(y, t)|^p) \tag{12}$$

$$= E \left(\left| \sum_{k \neq 0} \left[(c_k^{\frac{1}{2}} \int_0^t e^{K(t-s)} e^{\int_s^t dq} M_{t-s} db_s^k \right. \right. \right. \tag{13}$$

$$\left. \left. \left. + d_k \int_0^t e^{K(t-s)} e^{\int_s^t dq} M_{t-s} |k|^{\frac{1}{3}} ds \right) (e_k(x) - e_k(y)) \right|^p \right)$$

$$= E_b \left(\left(\sum_{k \neq 0} \left[(c_k^{\frac{1}{2}} \int_0^t e^{K(t-s)} |k|^{-\tau_p} E_B(M_{t-s}) db_s^k \right. \right. \right. \tag{14}$$

$$\left. \left. \left. + d_k \int_0^t e^{K(t-s)} |k|^{-\tau_p} E_B(M_{t-s}) |k|^{\frac{1}{3}} ds \right) \times 2e^{\pi k i(x+y)} \sin(\pi k \cdot (x - y)) \right|^p \right).$$

Now, we compute the action of the time average of the operator K on the Fourier components (eigenfunctions of \tilde{K}), replacing it with the eigenvalues $\lambda_k = C|k|^{\frac{2}{3}} + 4\nu\pi^2|k|^2$, see Birnir (2013b). This assumes that the expectation of the norm of u in the Sobolev space $H^{\frac{11}{6}+}$ is finite, see Lemma 2.7 in Birnir (2013b).

M_t is the exponential martingale:

$$M_t = \text{Exp} \left[\int (U + u) \cdot dB_s - \int \frac{|U + u|^2}{2} ds \right],$$

where $B_t \in \mathbb{R}^3$ is an auxiliary Brownian motion and $U + u$ is the Reynolds decomposition of the flow. A simple application of Ito’s formula yields

$$M_t^p = 1 + \int_0^t (U + u) M_s \cdot dB_s + \frac{p(p-1)}{2} \int_0^t |U + u|^2 M_s^p ds.$$

Thus, we have

$$E_B[M_t^p] = 1 + \frac{p(p-1)}{2} \int_0^t E_B[|U + u|^2 M_s^p] ds$$

$$\leq 1 + \frac{p(p-1)}{2} \int_0^t \sup_x |U + u|^2 E_B[M_s^p] ds.$$

Thus, by Grönwall’s inequality,

$$E_B[M_t^p] \leq e^{\frac{p(p-1)}{4} \int_0^t \sup_x (|U|^2 + |u|^2) dt}.$$

The sup in x frees the expectation from the expectation of the auxiliary Brownian motion, used to define the Martingale, and the exponent of the right-hand side is easily estimated by the same methods as below

$$E_b \left[\sup_x (|U|^2 + |u|^2) \right] \leq \sup_x |U|^2 + \frac{1}{C^2} \sum_{k \neq 0} \frac{(C/2)c_k + d_k^2}{|k|^{\zeta_2}} = \text{Constant}.$$

This implies that $E_B[M_t^P]$ only adds a constant, first to the exponents and then to the denominators, in the structure functions below and we will ignore it.

Finally, we take the absolute value and expand the polynomial expression in (12). To ultimately compute the structure functions, we use Ito’s Lemma

$$E \left[\left(\int_S^T f(t, w) dB_t \right)^2 \right] = \int_S^T E[(f(t, w))^2] dt$$

to turn any even power of the stochastic integral into a deterministic integral, which can then be solved for using standard calculus. For odd powers, we use the fact that

$$E \left[\int_S^T f dB_t \right] = 0$$

to eliminate such terms. We then find the first-order structure function is given by

$$\begin{aligned} E(|u(x, t) - u(y, t)|) &= S_1(x, y, t) \\ &= \frac{2}{C} \sum_{k \in \mathbb{Z}^3 \setminus \{0\}} \frac{|d_k|(1 - e^{-\lambda_k t})}{|k|^{\zeta_1} + \frac{4\pi^2 v}{C} |k|^{\zeta_1 + \frac{4}{3}}} |\sin(\pi k \cdot (x - y))|, \end{aligned} \tag{15}$$

where $|\cdot|$ denotes the vector norm in \mathbb{R}^3 . The second-order structure function is given by

$$\begin{aligned} E(|u(x, t) - u(y, t)|^2) &= S_2(x, y, t) \\ &= \frac{4}{C^2} \sum_{k \in \mathbb{Z}^3} \left[(|\sin^2(\pi k \cdot (x - y))|) \right. \\ &\quad \times \left\{ \frac{\frac{C}{2} c_k (1 - e^{-2\lambda_k t})}{|k|^{\zeta_2} + \frac{4\pi^2 v}{C} |k|^{\zeta_2 + \frac{4}{3}}} \right. \\ &\quad \left. \left. + \frac{|d_k|^2 (1 - e^{-\lambda_k t})}{|k|^{\zeta_2} + \frac{8\pi^2 v}{C} |k|^{\zeta_2 + \frac{4}{3}} + \frac{16\pi^4 v^2}{C^2} |k|^{\zeta_2 + \frac{8}{3}}} \right\} \right] \end{aligned} \tag{16}$$

where $c_k = |c_k^{\frac{1}{2}}|^2$. The third-order structure function is given by

$$\begin{aligned}
 E(|u(x, t) - u(y, t)|^3) &= S_3(x, y, t) \\
 &= \frac{8}{C^3} \sum_{k \in \mathbb{Z}^3} \left[(|\sin^3(\pi k \cdot (x - y))|) \right. \\
 &\quad \times \left\{ \frac{C}{2} c_k |d_k| (1 - e^{-2\lambda_k t})(1 - e^{-\lambda_k t}) \right. \\
 &\quad \times \left. \left[\frac{8\pi^2 v}{C} |k|^{\zeta_3 + \frac{4}{3}} + \frac{16\pi^4 v^2}{C^2} |k|^{\zeta_3 + \frac{8}{3}} \right. \right. \\
 &\quad \left. \left. + \frac{|d_k|^3 (1 - e^{-\lambda_k t})^3}{|k|^{\zeta_3} + \frac{12\pi^2 v}{C} |k|^{\zeta_3 + \frac{4}{3}} + \frac{48\pi^4 v^2}{C^2} |k|^{\zeta_3 + \frac{8}{3}} + \frac{64\pi^6 v^3}{C^3} |k|^{\zeta_3 + 4}} \right] \right\} \Big] \tag{17}
 \end{aligned}$$

The general p th order structure function is given by

$$S_p(x, y, t) = \frac{2^p}{C^p} \sum_{k \neq 0} A_p \times |\sin^p[\pi k \cdot (x - y)]|, \tag{18}$$

where

$$A_p = \frac{2^{\frac{p}{2}} \Gamma\left(\frac{p+1}{2}\right) \sigma_k^p {}_1F_1\left(-\frac{1}{2}p, \frac{1}{2}, -\frac{1}{2}\left(\frac{M_k}{\sigma_k}\right)^2\right)}{|k|^{\zeta_p} + \frac{p k \pi^2 v}{C} |k|^{\zeta_p + \frac{4}{3}} + \mathcal{O}(v^2)}, \tag{19}$$

where Γ is the gamma function, ${}_1F_1$ is the hypergeometric function, $M_k = |d_k|(1 - e^{-\lambda_k t})$, $\sigma_k = \sqrt{\left(\frac{C}{2} c_k (1 - e^{-2\lambda_k t})\right)}$, and p_k is different for each denominator term in the series. Note that the Reynolds number dependence is captured via the viscosity term v . C is a constant approximating the (Sobolev) norm of the small-scale velocity of the flow. It will be allowed to vary across structure functions to accommodate a relative change in the mean and the large deviations.

The above formulas clearly distinguish the stochastic closure theory (SCT) from previous theories on turbulence. SCT shows that the correct basis for the p th structure function, in Fourier space, is the collection of sine components of the lag variable, indexed by different wavenumbers and raised to the power p . The coefficients for this basis are given by formula (24). This allows us to represent all structure functions as functions of the lag variable for all Reynolds numbers and all powers p . Furthermore, this model is directly derived from the Navier–Stokes equations. Such a result has been unattainable until now. It permits a complete characterization of the experimental data for the structure functions in homogeneous turbulence.

4.1 The One-Dimensional Structure Functions

We want to fit the structure functions (23) to the experimental data collected in the VDTT. To do this, we have to reduce the three-dimensional structure functions to

one-dimensional ones, which are easier to obtain. We will perform the reduction in this subsection.

We consider structure functions where the measurements are taken at two distinct points along the length of the tunnel, in the direction of the mean velocity. These are called the longitudinal structure functions, $S_p(r, t)$, where $r = x - y$ is a vector along the main axis of the tunnel. One can also consider the transversal structure functions, $S_p(q, t)$, where $q = x - y$ is a vector in the radial direction of the tunnel, perpendicular to r . In homogeneous turbulence, these two structure functions are not independent. Their correlation matrix is given by Pope (2000):

$$D_{ij} = E [(u_i(x, t) - u_i(y, t))(u_j(x, t) - u_j(y, t))] \\ = S_2(r, t)I + (S_2(r, t) - S_2(q, t)) \frac{r_i r_j}{r^2},$$

where I is the identity matrix in $\mathbb{R}^3 \times \mathbb{R}^3$, and

$$S_2(q, t) = S_2(r, t) + r \frac{\partial}{\partial r} S_2(r, t),$$

with $r = |r|$, $|\cdot|$ denoting the vector norm in \mathbb{R}^3 . For $\eta \ll r$, D_{ij} is expected to reduce to

$$D_{ij} = C_2(\epsilon r)^{2/3} \left(\frac{4}{3} I - \frac{1}{3} \frac{r_i r_j}{r^2} \right).$$

Thus, in \mathbb{R}^3 , the correlation matrix is determined by longitudinal structure function $S_2(r, t)$ alone and we will restrict our attention to the longitudinal structure functions.

Consider the longitudinal third-order structure function given by the SCT:

$$S_3(r, t) = \frac{8}{C^3} \sum_{k \in \mathbb{Z}^3} \left[(|\sin^3(\pi k \cdot r)|) \left\{ \frac{C}{2} c_k |d_k| (1 - e^{-2\lambda_k t})(1 - e^{-\lambda_k t}) \right. \right. \\ \left. \left. + \frac{|d_k|^3 (1 - e^{-\lambda_k t})^3}{|k|^{\zeta_3} + \frac{12\pi^2 \nu}{C} |k|^{\zeta_3 + \frac{4}{3}} + \frac{48\pi^4 \nu^2}{C^2} |k|^{\zeta_3 + \frac{8}{3}} + \frac{64\pi^6 \nu^3}{C^3} |k|^{\zeta_3 + 4}} \right\} \right],$$

where $c_k = c_1 + c_2 + c_2$, $|d_k| = \sqrt{d_1^2 + d_2^2 + d_2^2}$ and $|k| = \sqrt{k_1^2 + k_2^2 + k_2^2}$, and $r = x - y$. If we take $r = (r, 0, 0)$ to lie along the axis of the VDTT (cylinder), then $r \cdot k = (rk_1, 0, 0)$, and since only the components with $x - y = (r, 0, 0)$ can be present in the sum, all the terms drop out except those with $k_2 = 0$ and $k_3 = 0$. Thus, $k = (k_1, 0, 0)$ and the three-dimensional sum reduces to a one-dimensional one. If taken $t \rightarrow \infty$, we get the one-dimensional structure function

$$S_3(r, t) = \frac{8}{C^3} \sum_{k_1 \neq 0} \left[(|\sin^3(\pi k_1 r)|) \left\{ \frac{\frac{C}{2} c_{k_1} |d_{k_1}|}{|k_1|^{\zeta_3} + \frac{8\pi^2 v}{C} |k_1|^{\zeta_3 + \frac{4}{3}} + \frac{16\pi^4 v^2}{C^2} |k_1|^{\zeta_3 + \frac{8}{3}}} \right. \right. \\ \left. \left. + \frac{|d_{k_1}|^3}{|k_1|^{\zeta_3} + \frac{12\pi^2 v}{C} |k_1|^{\zeta_3 + \frac{4}{3}} + \frac{48\pi^4 v^2}{C^2} |k_1|^{\zeta_3 + \frac{8}{3}} + \frac{64\pi^6 v^3}{C^3} |k_1|^{\zeta_3 + 4}} \right\} \right], \quad (20)$$

because $\zeta_3 = 1$, where $c_{k_1} = c_{(k_1, 0, 0)}$, $|d_{k_1}| = |d_{(k_1, 0, 0)}|$.

The argument for all the structure functions S_p , $p \geq 1$, is similar. We will compare the one-dimensional structure function with experimental data and drop the subscript 1 on k_1 . Thus, the general p th one-dimensional longitudinal structure function, in the stationary state, is given by

$$S_p(r, \infty) = \frac{2^p}{C^p} \sum_{k \neq 0} \frac{2^{\frac{p}{2}} \Gamma\left(\frac{p+1}{2}\right) \sigma_k^p {}_1F_1\left(-\frac{1}{2}p, \frac{1}{2}, -\frac{1}{2}\left(\frac{M_k}{\sigma_k}\right)^2\right)}{|k|^{\zeta_p} + \frac{p k \pi^2 v}{C} |k|^{\zeta_p + \frac{4}{3}} + \mathcal{O}(v^2)} |\sin^p[\pi k r]|, \quad (21)$$

where r and k are one dimensional, Γ is the gamma function, ${}_1F_1$ is the hypergeometric function, $M_k = |d_k|$, $\sigma_k^2 = \frac{C}{2} c_k$, and p_k is different for each denominator term in the series. Note that the Taylor–Reynolds number dependence is captured via the viscosity term v , as the Taylor–Reynolds number is given by $U\lambda/v$. C is a constant approximating the mean velocity fluctuation of the flow.

In order for the sum in $S_2(r, \infty)$ above, to converge, $c_k \sim \frac{1}{k^{1+\epsilon}}$. A similar argument applies to $\sum_{k \in \mathbb{Z} \setminus \{0\}} |d_k|$ in $S_1(r, \infty)$. For this reason, we expect the exponent m of k below to satisfy $m > 1$. We will in fact make the ansatz,

$$c_k = \sqrt{\frac{2}{\pi}} \frac{b}{b^2 + k^m}, \quad d_k = \sqrt{\frac{2}{\pi}} \frac{a}{a^2 + k^m}, \quad (22)$$

where c_k and d_k are the one-dimensional versions of the coefficients in the structure functions, to approximate the experimental data. Provided that m is greater than 1, the series determining the one-dimensional restriction of the structure functions (21) will converge. The thinking here is that there is a universal coefficient m for each Reynolds number that will determine how fast the sine series converges, and thus the spatial smoothness of the structure functions. Thus, for k large, c_k and $d_k \sim \frac{1}{k^m}$. Moreover, we are (optimistically) assuming that the two contributions c_k and d_k , to the large eddies, also scale with the order of the structure functions and can be characterized by a number b , respectively, a , for each Taylor–Reynolds number. Thus, for k small, $c_k \sim \frac{1}{b}$ and $d_k \sim \frac{1}{a}$. This turns out to work reasonably well, see Table 5.

In summary, we reduced the coefficients for the three-dimensional structure functions, c_k and d_k , to the ones for the one-dimensional structure functions, c_k and d_k , with $k = (k_1, 0, 0)$. We then fit the formulas for the one-dimensional structure functions to the data and propose a simple ansatz (22), for the coefficients' dependence on the Taylor–Reynolds number and the wavenumber $1/k$.

Table 1 Here, η is the Kolmogorov length scale given in micrometers, L is the integral length scale given in millimeters, and ν is the viscosity given in m^2/s

Taylor–Reynolds number	η	L	ν
110	1025	165.1	$1.55(10^{-5})$
264	162	102.5	$2.34(10^{-6})$
508	91	123.9	$1.00(10^{-6})$
1000	36	136.6	$2.91(10^{-7})$
1450	22	129.5	$1.50(10^{-7})$

The data here are at the furthest measured point downstream of the grid, as η and L evolve downstream

5 Comparison of the Model with the Data

The VDTT is capable of using pressurized inert gases as working fluids. Specifically, the use of pressurized sulfur hexafluoride with a low kinematic viscosity enables classical grid experiments at R_λ up to 1600. The turbulence in the VDTT was generated by a fixed grid of crossed bars and is called classical grid turbulence (Comte-Bellot and Corrsin 1966; Corrsin 1961). The classical grid disturbed the free flow mechanically at the upstream end of the test section. In the wake of the grid, the turbulence evolved along the length of the tunnel without the middle region being substantially influenced by the walls of the tunnel (Bodenschatz et al. 2014). The measurements were made with a Dantec StreamLine hot-wire anemometry system, using NSTAPs developed at Princeton University, see Vallikivi and Smits (2014). The hot-wire probes were at a distance of 7.1 m downstream from the 186.6 mm classical grid, so that the turbulence evolved through at least one eddy turnover time. Taylor’s frozen flow hypothesis is used to extract x and r from the time series of the probe as in Bodenschatz et al. (2014). Measurements were taken for Taylor–Reynolds numbers 110, 264, 508, 1000 and 1450. The pertinent parameters for the data are given in Table 1. For more information about the experiments, see Sinhuber et al. (2015, 2017). Each measurement was taken over five minutes and sampled at 60kHz, giving $1.8(10^7)$ data points.

The longitudinal velocity differences are

$$\delta u(r, t) = u(y, t) - u(x, t) = u(x + r, t) - u(x, t)$$

where x and r are parallel vectors along the x -axis. The system length in the tunnel is an important value when fitting the data since we scale the lag variable, $\frac{r/\eta}{\text{system length}} = (x - y)$, with the system length. The system length in our case is the mesh size of the grid, and not the square root of the cross-sectional area of the tunnel, for instance. The structure functions were plotted against r/η , where r is the distance between positions x and y as given by the Taylor frozen flow hypothesis and η is the Kolmogorov length scale. In order for our sine series formula to capture the entire data set, we divided r/η by its maximum value for which we computed structure functions, which was $\frac{r}{\eta} = 19540$. We also introduced a variable, D , so that we substituted

$$\frac{r}{\eta}/(19540(D))$$

Table 2 The fitted values for A_1 in Eq. (25)

Re_λ	110	264	508	1000	1450
Second order	0.00744	.0153	.0169	.0183	.0195
Third order	.00154	.00395	.00484	.00564	.00664
Fourth order	.000384	.00189	.00228	.00251	.00305
Sixth order	.0000341	.000431	.000566	.000552	.000691
Eighth order	$3.12(10^{-6})$.0000839	.000122	.000144	.000204

Table 3 The fitted values for A_2 in Eq. (25)

Re_λ	110	264	508	1000	1450
Second order	.00285	.00583	.00653	.00697	.00666
Third order	.000872	.00299	.00526	.00488	.00395
Fourth order	.000174	.000746	.000804	.001	.0006
Sixth order	$4.24(10^{-6})$	−.0000756	−.00011	.0000919	.0000654
Eighth order	$1.04(10^{-6})$.0000127	.0000147	.0000264	− $4.71(10^{-7})$

for $x - -y$ in the formulas. The fitted values for D are given in Table 5. Note that D is one of the four parameters which are not active over the range of Taylor–Reynolds numbers, which are shown in Fig. 6 and will be justified later.

5.1 VDTT Dependent Fits: Grid and Large Eddies, Mean Small-Scale Velocity

We need to allow for variation in the non-universal largest scales of the flow (Blum et al. 2011). This is experiment specific and influences only the first two terms of the sine series. These parameters are only significant for low Reynolds numbers, see Tables 2 and 3. This clearly distinguishes these two parameters from the others. As a result, we see that the grid can stimulate the first two sinusoidal modes but does not influence the rest of the cascade. Thus, the SCT formula becomes:

$$S_p(x, y, t) = A_1 \sin[\pi|x - y|] + A_2 \sin[2\pi|x - y|] + \frac{2^p}{C^p} \sum_{k=3} A_p \times |\sin^p[\pi k|x - y|]|, \tag{23}$$

where

$$A_p = \frac{2^{\frac{p}{2}} \Gamma\left(\frac{p+1}{2}\right) \sigma_k^p {}_1F_1\left(-\frac{1}{2}p, \frac{1}{2}, -\frac{1}{2}\left(\frac{M_k}{\sigma_k}\right)^2\right)}{|k|\zeta_p + \frac{pk\pi^2\nu}{C}|k|\zeta_p + \frac{4}{3} + \mathcal{O}(\nu^2)}, \tag{24}$$

and A_1 and A_2 are the free parameters. The first two terms capture the interaction of the grid and the two largest eddies in the flow. However, this influence is limited to the

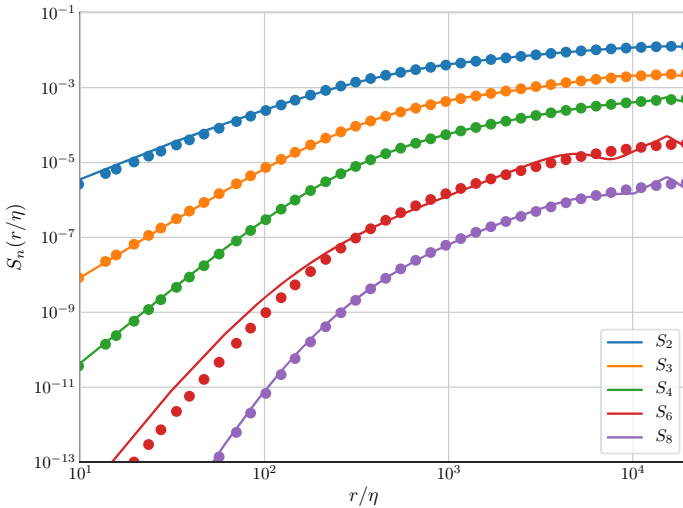


Fig. 1 Taylor–Reynolds number 110. Note that the plots are made on a log–log scale. The dots correspond to the data from the VDTT, whereas the line is the fitted SCT

lowest Reynolds numbers and becomes insignificant for the higher Reynolds numbers and the modeling range of the rest of the parameters.

Fitting was done in Mathematica using the built-in “findfit” function. To bound computational time reasonably, the series given in Sect. 2 were limited to one thousand terms. The full model used to fit the data is given by

$$\begin{aligned}
 S_p = & A_1 |\sin[(\pi r/\eta)/(19540.3(D))]| + A_2 |\sin^2[(2\pi r/\eta)/(19540.3(D))]| \\
 & + \sum_{k=3}^{2^p} \frac{2^p}{C^p} A_p |\sin^p[(\pi k r/\eta)/(19540.3(D))]|, \tag{25}
 \end{aligned}$$

where A_p is given by (24). The fits are done with seven parameters, namely a , b , m , C , D , A_1 and A_2 . The fits are shown in Figs. 1, 2, 3, 4, 5. However, only three parameters are active over the entire inertial range, specifically a , b and m , in the sense that they are changing the relative weights of the Fourier components of the solution $u(x, t)$. The parameter D measures the system length correction for large Reynolds numbers. This correction serves to place the transition from the dissipative range to the inertial range. The parameter C measures the root-mean-squared small-scale velocity, whereas A_1 and A_2 measure the influence of the large eddies upon the grid. These three parameters measure the transition out of the inertial range. This is shown in Figs. 6, 7 and 8 and will be justified later. The best results came when using the fourth-order structure functions for each Taylor–Reynolds number to fix the coefficients a , b and D .

Tables 2, 3 and 4 contain the fitted values of A_1 , A_2 and C respectively, as described in (25). Note that A_1 , A_2 , C and m are given their own tables as they change with the order of the structure function, whereas a , b and D are placed in the same table as they do not. Consider Fig. 9a that shows the values of the coefficient A_1 as a

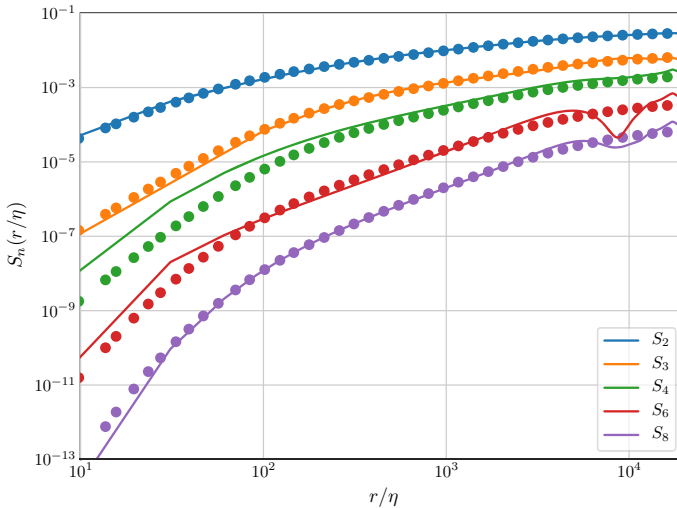


Fig. 2 Taylor–Reynolds number 264. Note that the plots are made on a log–log scale. The dots correspond to the data from the VDTT, whereas the line is the fitted SCT

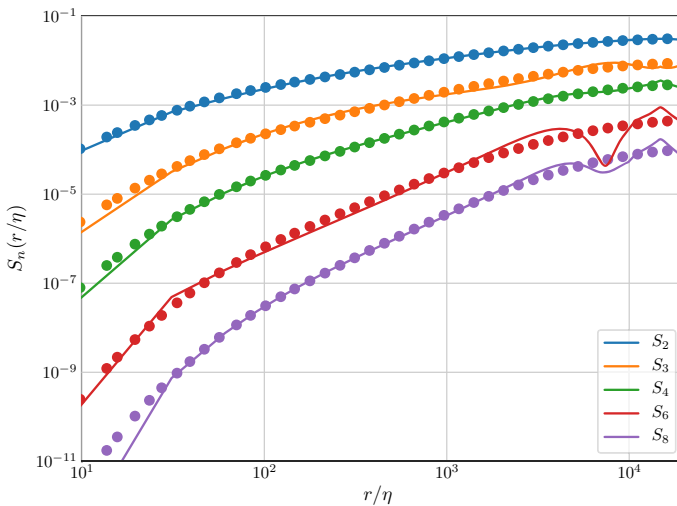


Fig. 3 Taylor–Reynolds number 508. Note that the plots are made on a log–log scale. The dots correspond to the data from the VDTT, whereas the line is the fitted SCT

function of the Taylor–Reynolds number taken from Table 2. We show that the values are small and do not change much over the range of T–R numbers in the experiment. The figure shows the values based on the first three structure functions do not change much of the whole over the range of T–R numbers in the experiment and the higher-order structure functions give negligible correction. One can think of the second-order structure function as the root-mean-square size of the largest eddy in the flow. Table 3 shows that the same analysis applies to the coefficient A_2 except that its values are

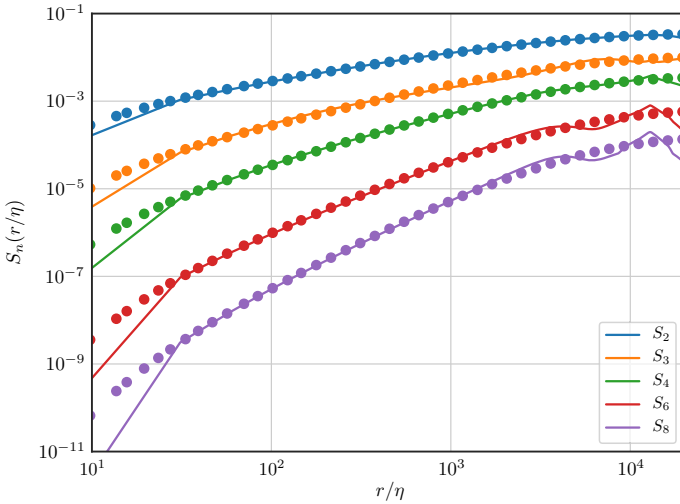


Fig. 4 Taylor–Reynolds number 1000. Note that the plots are made on a log–log scale. The dots correspond to the data from the VDTT, whereas the line is the fitted SCT

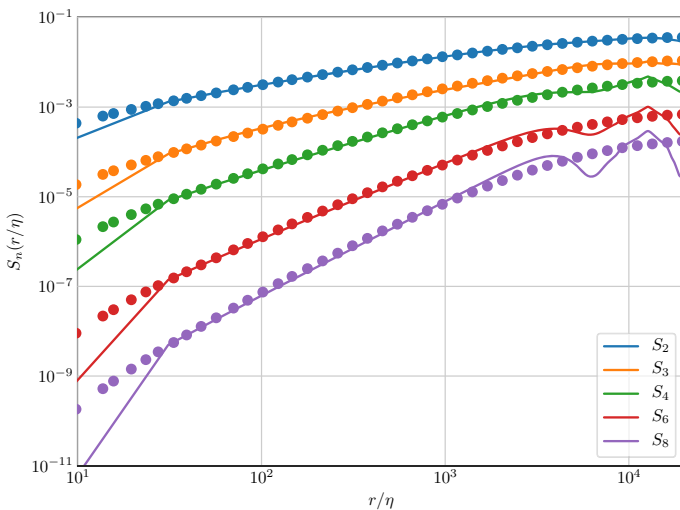


Fig. 5 Taylor–Reynolds number 1450. Note that the plots are made on a log–log scale. The dots correspond to the data from the VDTT, whereas the line is the fitted SCT

even smaller. Consequently, we omit the plot of A_2 . Table 4 shows that the parameter C increases over the range of T–R numbers in the experiment and Fig. 9b shows its plot corresponding to the increasing structure functions. We see that only the second moment (red), measuring the root-mean-square size of the mean fluctuation velocity, increases significantly over the range of T–R numbers in the experiment, see Fig. 9b. The plots corresponding to the higher moments increase significantly less, although they indicate that the mean velocity is getting spatially rougher. However, this is not

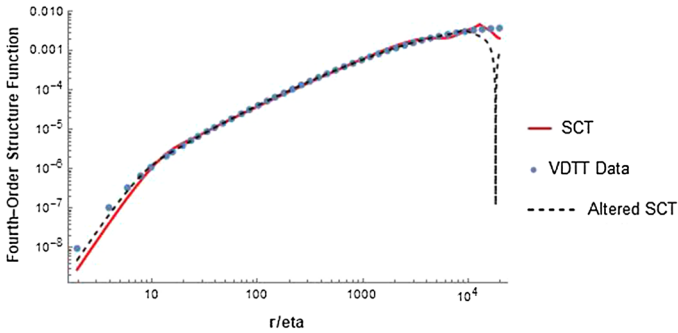


Fig. 6 The two different fits for Taylor–Reynolds number 1450. The red solid line corresponds to the previously given fit with $D = 1.3$, whereas the black dashed line corresponds to the fit with $D < 1$. Note the downward peak for the black dashed line resulting from the sine series wanting to return to zero before the last data point (Color figure online)

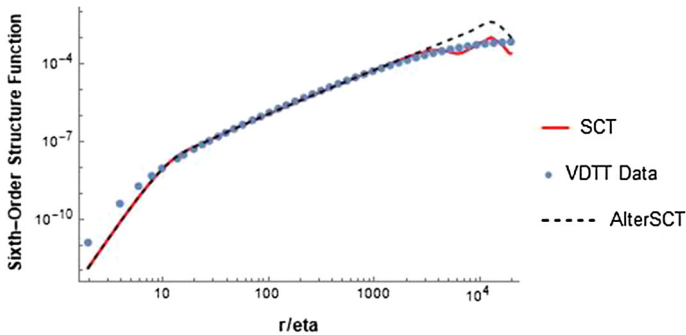


Fig. 7 The original fit to the sixth-order structure function for Reynolds number 1450 is the red solid line. The black dashed line is if we tie A_1 and A_2 back to the original formula (23). Note the effect on the largest values of r/η and how this creates the wiggles we are seeing (Color figure online)

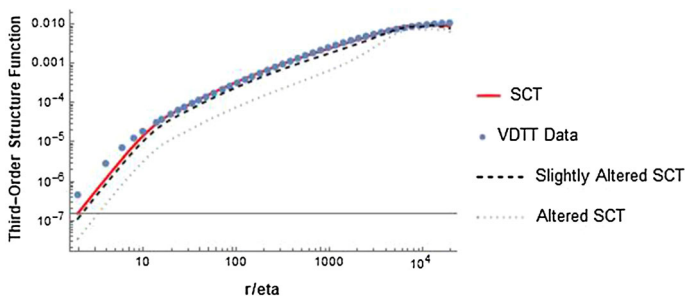


Fig. 8 The red solid line is the original fit to the third-order structure function for Reynolds number 1450. The black dashed line changes the value of the parameter C from 3.59 to 4. Note the effect here, as the original fit for the dissipative and inertial range is pushed down slightly, and a new transitional regime is created. This effect is more pronounced in the brown dotted line, when C is increased from 4 to 6 (Color figure online)

Table 4 The fitted values for C in Eq. (25)

Re_λ	110	264	508	1000	1450
Second order	2.8	3.31	4.21	7.62	21.1
Third order	1.4	1.27	1.49	2.72	3.59
Fourth order	1.07	1.01	1.19	2.36	6
Sixth order	1.15	1.29	1.34	1.73	2.49
Eighth order	0.616	.531	.596	1.17	2.84

Table 5 The fitted values for a , b and D in Eq. (25)

Re_λ	a	b	D
110	11.64	0.01612	1.569
264	9.581	0.05236	1.769
508	8.314	0.06504	1.518
1000	3.792	0.09247	1.32
1450	2.684	0.4092	1.3

Note that these parameters are grouped as they are independent of the order of the structure functions

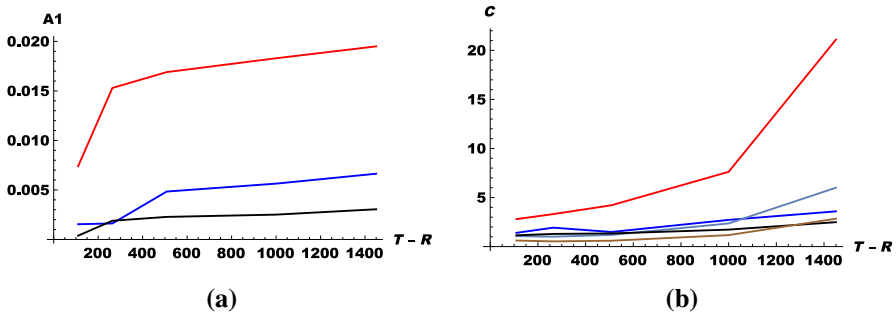


Fig. 9 **a** The values of the coefficient A_1 of the first Fourier component, as a function of the Taylor–Reynolds number, from Table 2. Top (red) second moment, second from top (blue) third moment, third from top (black) fourth moment. The higher moments give negligible correction, whereas the first three change little, notice the scale, over the range of T–R numbers in the experiment. **b** The values of the coefficient C , as a function of the Taylor–Reynolds number, from Table 4, top (red) second moment (root-mean-square size), lower, the higher moments. Notice that neither (a) or (b) is plotted on a log scale (Color figure online)

influencing much the balance of the Fourier components in the Fourier representation of $u(x, t)$ compared to the significant changes in the parameters a , b and m discussed below. It simply measures the increase in the mean turbulent velocity as the turbulence increases. One can interpret this as a consequence of the fact that the turbulence in the VDTT is homogeneous but not fully isotropic. Thus, even with constant fan speed, the mean small-scale velocity increases with Reynolds number (increased by changing the pressure). The top line in Table 4 expresses this most clearly.

Table 5 shows the parameter D (measuring system size) does not change with the order of the structure functions and does not change much over the range of T–R numbers in the experiment.

The conclusion of the analysis of the parameters D , A_1 , A_2 and C in this section is that they are characteristics for the VDTT and the experiment. The first three do not change much with Reynolds number, and D is a small tuning of the system size that is necessary for capturing the influence of the grid. A_1 and A_2 are the amplitudes of the first two large eddies in the flow, presumably influenced by the grid. They are only significant for low Reynolds number. We model them or the interaction of the grid and the first two eddies for small Reynolds number. C is the only parameter that increases with the Reynolds number. It measures the root mean square of the small-scale mean velocity, and since the flow is generated by a constant large-scale flow, C will increase with the Reynolds number as measured by the second structure functions. This small-scale mean flow can be considered to be the result of the non-isotropy of the flow. The higher-order structure function measures the smoothness of the mean small-scale flow and does not change much with Reynolds number, see Table 4 and Fig. 9b. Thus, these four parameters are VDTT specific and not universal for homogeneous turbulence, in distinction to the remaining parameters a , b and m , discussed in the next section, that all change with Reynolds number and are we believe universal for homogeneous turbulence and independent of the VDTT.

6 Evaluation of the Model

In this section, we present the results of the fits to the data. In Figs. 1, 2, 3, 4 and 5, the dots are the data from the experiment, while the lines are the SCT theory predictions. The agreement between the theory is satisfactory for most orders of the structure functions and for most Reynolds numbers. For the highest Reynolds numbers and highest-order (sixth and eighth order) structure functions, we see differences between the theory and experiment at the smallest scales. In general, we note that the fits become less accurate as we increase the order of the structure functions. The fits for the second-, third- and fourth-order structure functions are generally better than the fits for the sixth- and eighth-order structure function fits, which are rougher. This is expected from the theory given by Birnir (2013b) and will be explored further in a future paper (Fig. 6).

6.1 VDTT Independent Fits: Homogeneous Turbulence

Table 5 gives the fitted values for a and b that change significantly over the range of T–R numbers in the experiment, see Fig. 10. This table shows that the central limit theorem term,

$$\bar{D} = \sum_{k \neq 0} c_k^{\frac{1}{2}} db_t^k e_k(x); \quad c_k^{\frac{1}{2}} = \sqrt{\frac{2}{\pi}} \frac{b}{b^2 + k^m},$$

as given by b has a greater influence for smaller Taylor–Reynolds numbers than the large deviation principle term:

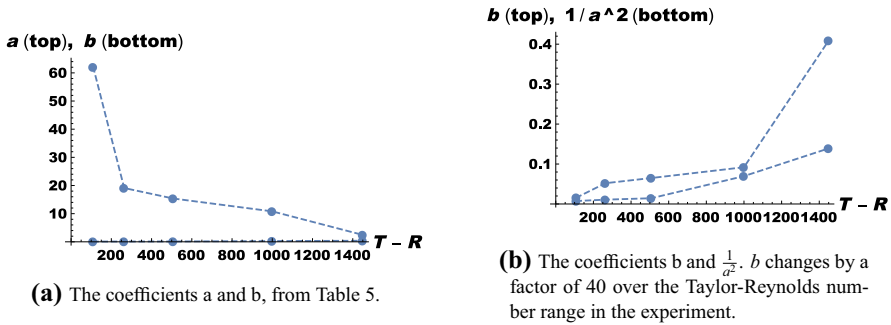


Fig. 10 The dependence of the coefficients, in the improved SCT model (26), on the Taylor–Reynolds number. The coefficient $\frac{1}{a^2}$ makes the large deviation contribution in (26), so it is plotted separately against b . Note that a versus b is included for completeness but due to the nature of the Fourier coefficients c_k and d_k as defined in (22), the ideal comparison is b against $\frac{1}{a^2}$

Table 6 The fitted values for m in Eq. (25)

Re_λ	110	264	508	1000	1450
Second order	1.563	1.16	1.069	.8965	.9148
Third order	1.408	1.111	0.922	.6488	.5262
Fourth order	1.269	.8751	.7936	.5554	.4865
Sixth order	.98607	.5055	.5192	.4339	.3398
Eighth order	.9711	.5924	.5755	.3771	.2482

$$D' = \sum_{k \neq 0} d_k \eta_k dt e_k(x); \quad d_k = \sqrt{\frac{2}{\pi}} \frac{a}{a^2 + k^m},$$

given by a , as for small values of k , these terms essentially become $\frac{1}{a^2}$ and b , respectively, because b is small. As the Reynolds number goes up, we do see an increasing influence of b dominating the increase of $\frac{1}{a^2}$, see the plot in Fig. 10b. Thus, the contribution of the central limit theorem is greater.

We do not have enough data to tell what the limits of a and b are as the Taylor–Reynolds number R_λ goes to infinity. Table 5 shows that b increases with R_λ presumably reaching a limit $b(\infty) < 1$, and a decreases with R_λ probably going to a limit $a(\infty) > 1$. Below we will show that a is more influential than b as R_λ becomes large.

The values of the exponent m of the wavenumber $k = k_1$ are given in Table 6. Their change over the inertial range seems small, but since m is an exponent, the influence on the weight of the Fourier components of $u(x, t)$ is highly significant. In general, the exponents are larger or very close to 1, at least near the top of the table. The first (top) line in Table 6, corresponding to the second-order structure function, verifies the hypothesis concerning the coefficients c_k and d_k in Sects. 2 and 4. The one-dimensional coefficient c_k and d_k , from Sect. 4.1, should decay as $|k|^{-m}$, $m > 1$. All the exponents in the first line in Table 6 satisfy this except the last two. However, both still lie within the fitting uncertainty and may be explained by the Reynolds

number corrections absorbing the weight of the power. Thus, the exponents $m(R_\lambda)$ in the first line depend on R_λ , but approach 1 as R_λ becomes large. We would expect the exponents to remain above one for the rest of the lines on the table, but this is not the case. We will seek to explain this result in a future paper.

7 The Improved SCT Model

The comparison of theory and data for homogeneous turbulence now produces a much improved stochastic closure model, removing the infinitely many coefficients c_k , d_k and h_k from Eq. (7). What we find is that the large scales satisfy Eq. (4), whereas the small-scale flow satisfies the stochastic Navier–Stokes equation:

$$\begin{aligned} du + u \cdot \nabla u dt &= (v \Delta u + \nabla(\Delta^{-1}[\text{Trace}(\nabla u)^2])) dt - u \cdot \nabla U - U \cdot \nabla u \\ &+ \sum_{k \neq 0} \left(\frac{\mathbf{a}}{|a|^2 + |k|^m} \right) |k|^{-\frac{5}{3}} dt e_k(x) \\ &+ \sum_{k \neq 0} \frac{\mathbf{b}^{1/2}}{(|b|^2 + |k|^m)^{1/2}} |k|^{-2} db_t^k e_k(x) \\ &- u \frac{1}{3} \sum_{k \neq 0} \bar{N}_t^k dt, \end{aligned} \quad (26)$$

where \mathbf{a} , $\mathbf{b}^{1/2}$, $k \in \mathbb{R}^3$, $a = |\mathbf{a}|$, and $b = |\mathbf{b}^{1/2}|^2$. The improved SCT model depends on three parameters a , b and m , which are all function of the Taylor–Reynolds number R_λ . A plot of a and b from Table 5 is shown in Fig. 10a. It shows that the large deviation coefficient a is larger than the central limit theorem coefficient b . But this is deceiving since the right comparison is between $1/a^2$ and b for small wavenumber k , because of the form of the coefficients c_k , d_k in (22). This comparison is shown in Fig. 10b. We see that b is larger than $1/a^2$ and dominates for small Reynolds numbers. For large wavenumbers k , b dominates even more because now it is compared with a^2/k^2 . The conclusion is that the central limit theorem term is the main contributor to the noise in the velocity differences, for small Reynolds numbers, and the bias given by the large deviation term is only significant for large Reynolds numbers. We will verify this below.

The coefficient C that appears in the computation of the structure functions (21) is not constant for each Taylor–Reynolds number, see Table 4, because it measures both the size of the velocity fluctuations and the relative strength of the center limit theorem term and the large deviation term in the noise. However, it does not vary much over the center part of Table 4 as a function of the Taylor–Reynolds number. The exponent m also varies with Taylor–Reynolds number. However, it also does not vary much with the Taylor–Reynolds number above the diagonal, as indicated by the bold numbers, in Table 6.

7.1 The Characterization of the Noise

We will now answer the question: “What is the noise in homogeneous turbulence?” based on the improvements of the SCT model. This is the question that is stated in Sect. 3 and partially answered by the original SCT model. We can completely answer the question and characterize the noise appearing in the stochastic Navier–Stokes equation (7). Recall that the original conjecture by Landau and Lifshits (1959) was that the noise was white or uncorrelated. The question can be rephrased to ask what the noise forcing is that the fluid velocity is subjected to in fully developed turbulence. In the stochastic Navier–Stokes equation, the noise was modeled (SCT) as a Fourier series with infinitely many coefficients, but now these coefficients have been determined by the experimental data in Sect. 5. The following observations can be made:

The Noise in Homogeneous Turbulence:

1. The color of the noise in the stochastic Navier–Stokes equation (7) depends on the Reynolds number through the coefficients a , b and the exponent m .
2. For small Reynolds number, the mean-field noise, or the central limit theorem and large deviation noise, is exponentially correlated (decaying), with correlation (Fig. 17):

$$C_r = \frac{C}{2} e^{-2\pi br} + \frac{1}{2} e^{-2\pi ar} \left(r + \frac{1}{2\pi a} \right),$$

up to a multiplicative factor of $\frac{1}{C^2}$, where the values of $b(Re_\lambda)$ (central limit theorem), $a(Re_\lambda)$ (large deviation) and $m(Re_\lambda)$ (spatial smoothness) are taken from Tables 4, 5 and 6, for low values of Re_λ , and $r = |x - y|$ is the correlation distance between two points x and y in the fluid, see Fig. 11a.

3. For large Reynolds number, the mean-field noise becomes oscillatory, approaching the correlation:

$$C_r = \frac{C}{2} b \cos(2\pi b^2 r) + 2\pi a^2 r \sin(2\pi a^2 r),$$

up to a multiplicative factor of $\frac{1}{C^2}$, again taking the values from Tables 4, 5 and 6, for high values of Re_λ , see Fig. 11b.

These correlations are computed using the variance of the velocity and the second-order structure function above, using the well-known formula $S_2(r) = 2(\sigma - C_r)$ and taking the limit of a very large spatial period. The exact formulas of the correlations depend on the ansatz that we made for the coefficients c_k and d_k in Sect. 4.1, but the above statements, about the nature of the correlations, are true in general. Thus, they represent the physical noise in the VDTT but more generally the generic noise in homogeneous turbulence.

Once we put in the values of b and a from Table 5, we see that the slow decay of $e^{-2\pi br}$ (central limit theorem) dominates for small Reynolds numbers, but the rapid oscillations of $2\pi a^2 r \sin(2\pi a^2 r)$ (large deviation) dominate for large Reynolds number. This is consistent with the observations made above. Recall, however, that

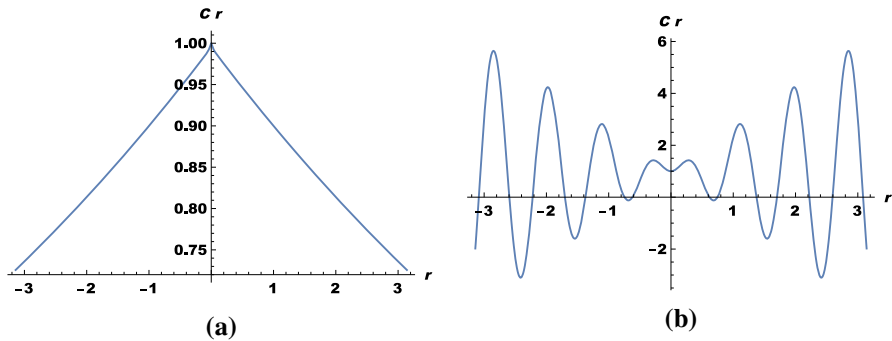


Fig. 11 **a** The normalized (Pearson's coefficient) two-point correlation, of the noise in the Navier–Stokes equation (26), for Taylor–Reynolds number 110, with values of a and b from the first line in Table 5, and C from the first column, first line of Table 4. **b** The normalized (Pearson's coefficient) two-point correlation, of the noise in the Navier–Stokes equation (26), for Taylor–Reynolds number 1450, with values of a and b from the last line in Table 5, and C from the last column, first line of Table 4

these are the correlations of the noise in the stochastic Navier–Stokes equation, not the correlations of the turbulent velocity itself, see Sect. 4.

Comparing with the conjecture made by Landau and Lifschitz in Landau and Lifshits (1959), we see that they were missing the Reynolds number dependance of the noise. However, their conjecture was not so far from the noise in homogeneous turbulence at large Reynolds numbers. It was only missing the rapid oscillations (growing with increasing lag variable) that enable the turbulent velocity to remain continuous.

8 Sensitivity Analysis

Now that we have compared the experimental data from the VDTT to formulas computed by the SCT, it is desirable to check how robust these results are. In particular, we want to know whether the formulas with the Reynolds number corrections do better than the formulas without them? Also, do the results depend on the probe size used in the experiments or are they independent of it? In this section, we perform a sensitivity analysis to test the results and answer these questions.

First, we consider the formula for the general p th structure function as given in (21). One way to let the Reynolds number go to infinity is to let the viscosity of the fluid go to zero. Doing so simplifies the coefficients A_p in (24), so that for $R_\lambda = \infty$, $\nu = 0$,

$$A_p = \frac{2^{\frac{p}{2}} \Gamma\left(\frac{p+1}{2}\right) \sigma_k^p {}_1F_1\left(-\frac{1}{2}p, \frac{1}{2}, -\frac{1}{2}\left(\frac{M_k}{\sigma_k}\right)^2\right)}{|k|^{\zeta_p}}. \quad (27)$$

The further denominator terms found in (26) but not above are corrections to the formula to account for the Reynolds number of the flow. Data fits were also done to the formula without the Reynolds number corrections. Figures 12, 13, 14, 15 and 16

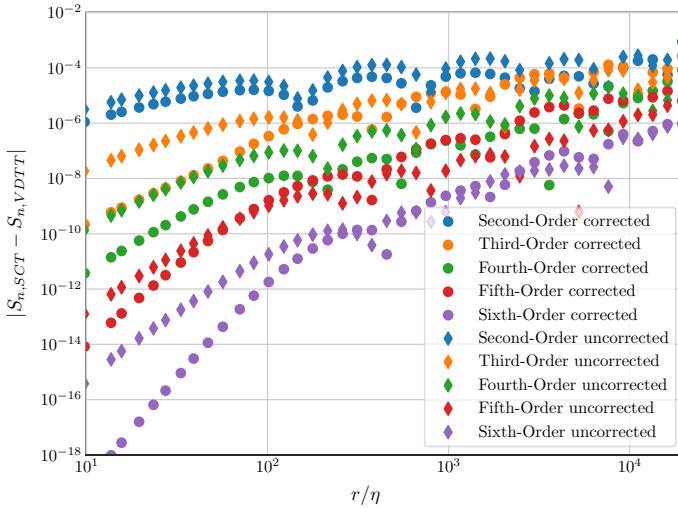


Fig. 12 Error for Taylor–Reynolds number 110. Note that the plots are made on a log–log scale

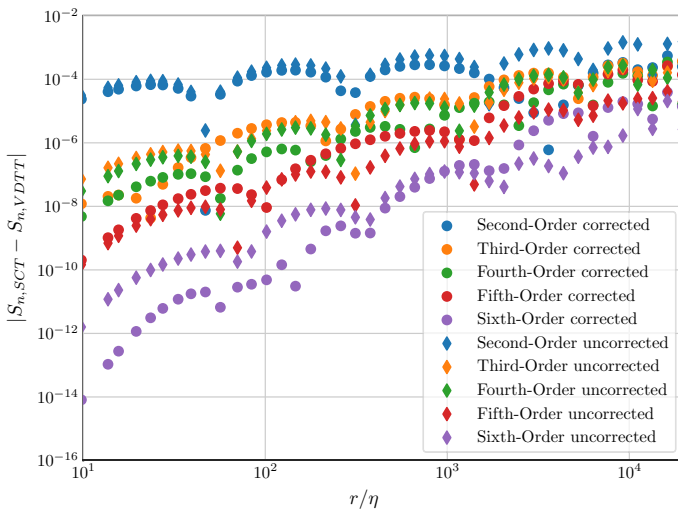


Fig. 13 Error for Taylor–Reynolds number 264. Note that the plots are made on a log–log scale

are plots of the error between the formula fits and the data at each data point. The changed values for the parameter m for the uncorrected fits is given in Table 7. The blue circles are the error to the Reynolds corrected formulas, while the red diamonds are the error to the formula without the Reynolds number correction.

There are a couple of observations to make about the error plot. First, for small Taylor–Reynolds numbers, it appears that the corrections improve the fitting, especially for the smaller data points. This improvement erodes as the Taylor–Reynolds number increases, until we see very little difference in accuracy for Taylor–Reynolds number 1450. This makes sense, as the corrections to account for Reynolds num-

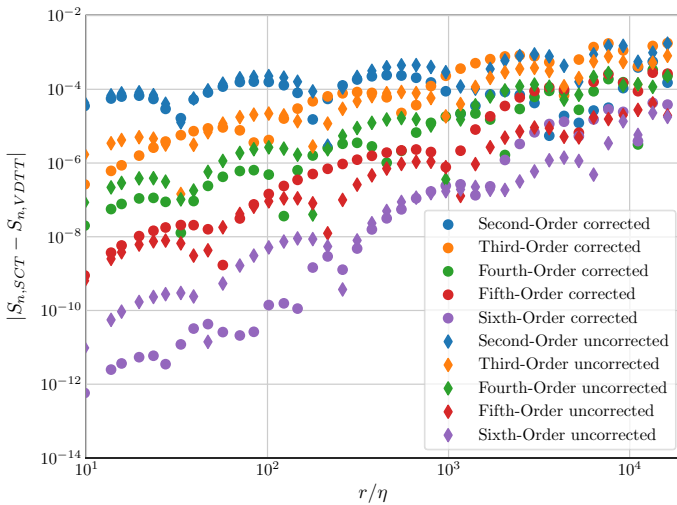


Fig. 14 Error for Taylor–Reynolds number 508. Note that the plots are made on a log–log scale

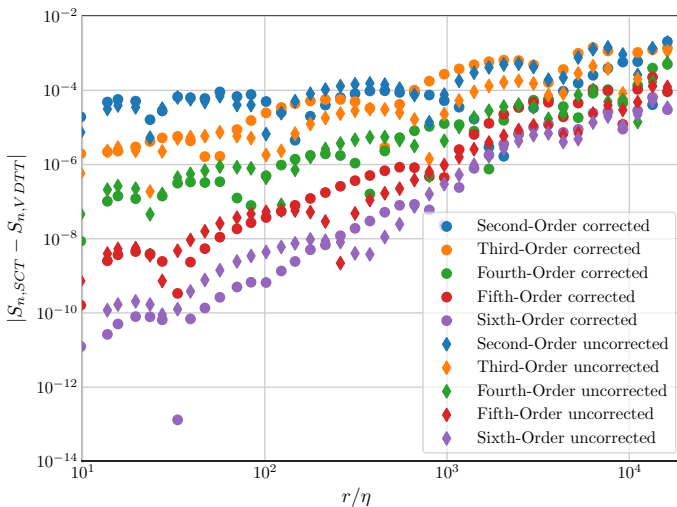


Fig. 15 Error for Taylor–Reynolds number 1000. Note that the plots are made on a log–log scale

ber get smaller as the Reynolds number increases, with the formulas becoming the uncorrected version when we let the Reynolds number go to infinity.

We also see an issue in fitting the smallest data points for solely for Reynolds number 1450. This issue appears to be connected to the system length, as shown in Fig. 6. A second fit to the fourth structure function for this Reynolds number was found with $D = .921$. This does improve the fitting for the smaller data points. However, D being this small causes an issue at the larger data points, namely the sine curve wants to return to zero before the last data point. Since there are relatively few data points at small values of r/η , we set $D = 1.3$. The value of 1.3 was chosen as it the

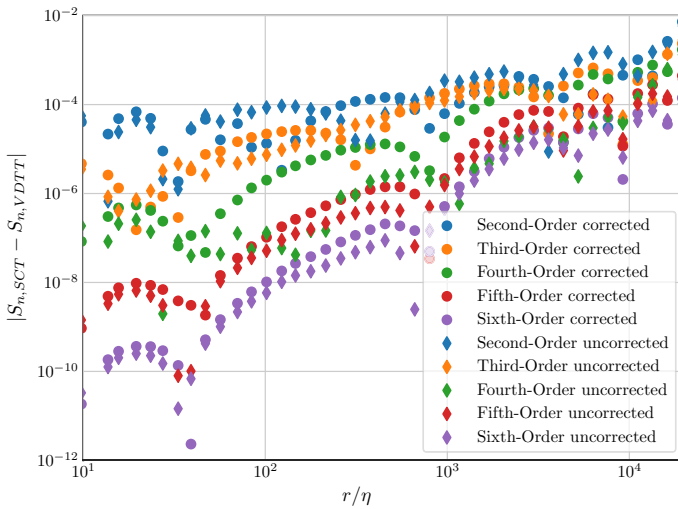


Fig. 16 Error for Taylor–Reynolds number 1450. Note that the plots are made on a log–log scale

Table 7 The fitted values for m for the uncorrected for Reynolds number effects structure function fits

Re_λ	110	264	508	1000	1450
Second order	2.09081	1.49402	1.31448	1.07963	0.984291
Third order	1.79012	1.41339	1.05553	0.822192	0.730565
Fourth order	1.6408	1.09179	0.920749	0.687336	0.595942
Sixth order	1.65727	1.08667	0.91658	0.681818	0.592901
Eighth order	1.66164	1.06728	0.901549	0.662111	0.577724

smallest number needed to fully capture the larger data points. Figure 6 also illustrates the effect D has on the fits, serving to place the transition from the dissipative range into the inertial range.

One potential point of concern with the fitting result was the probe size. The size of the probe could influence the fit, and a different probe size could produce different results. To check for this, fits were redone with a reduced number of data points. In particular, for every Taylor–Reynolds number and every structure function, fits were redone without including the first, the first two and the first three data points, respectively. We saw minimal change in the main parameters, the greatest being a difference of one in the third significant digit. The robust test for Reynolds number 508 is included in Fig. 17. As we can see, there is not a significant change in the value of m when removing the first couple of data points. However, the removal of fifteen or more data points removes the entire dissipative range and so we would expect the changes to be significant. As a result, we are convinced the fits are unaffected by the probe size.

Finally, we show the effect parameters A_1 , A_2 and C have on the fits. Figure 7 shows the effects of A_1 and A_2 . Note that these effects show up for all Reynolds number and

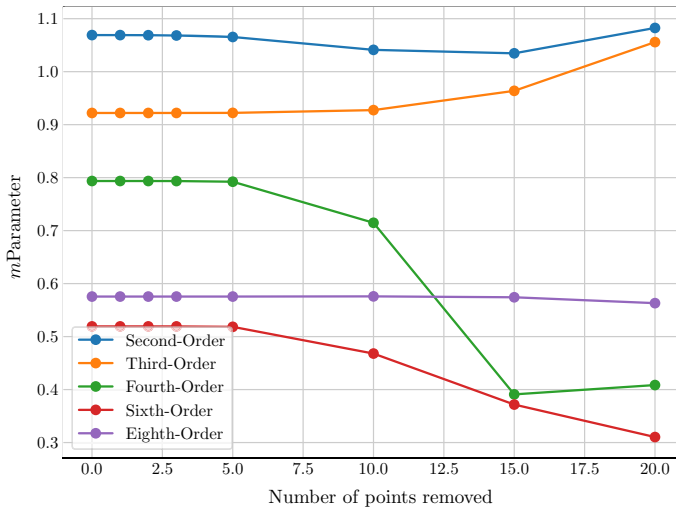


Fig. 17 Robustness test for a Reynolds number of 508. Note that the x -axis is the number of data points removed from the fitting. We see very little change in the m parameter until we remove enough data points to eliminate the dissipative range completely. Note the scales on the y -axis. As a result, we are convinced our fits are not dependent on the probe size

all order of structure functions, although they become negligible as the order of the structure function increases. These two parameters also created the wiggles we see at the largest values of r/η . Figure 8 shows the effect of parameter C . This parameter places the vertical location of the transition out of the inertial range.

9 Conclusion

We started by following Kolmogorov's method as described in Sect. 2 to close the Navier–Stokes equations that describe fully developed turbulence. We did this by introducing a stochastic forcing term to account for the small scales, see Birnir (2013a). Having closed the model, we then compute a sine series representation for the structure functions of turbulence, with Reynolds number corrections. These formulas were then fitted to data generated from the variable density turbulence tunnel at the Max Planck Institute for Dynamics and Self-Organization. The fits proved to be good with seven parameters. However, only three of these parameters a , b , m were active over the entire range of T–R numbers in the experiment, although one more parameter C measures the mean fluctuation velocity and increases over the range of T–R numbers in the experiment. Of the other four D , A_1 , A_2 and C , one D is active only for the transition from the dissipative range into the inertial range, whereas the other three are active for the transition out of the inertial range.

It thus seems that the parameters D , A_1 , A_2 and C are particular to the VDTT and experiments without isotropy, but the three parameters a , b and m are universal and characteristic for homogeneous turbulence. This obviously has to be tested by comparison with other experiments in homogeneous turbulence.

We also compared fits to the formula with a correction to account for the Reynolds number to fits without that correction. This difference is quantified in Figs. 12, 13, 14, 15 and 16. We see that the Reynolds correction formulas generate better fits as the Reynolds number increases for lower structure functions but have little impact on the fits for the higher structure functions.

Acknowledgements The experimental data presented in this paper were taken during the doctoral studies of Michael Sinhuber, group leader/postdoc during the time of Greg Bewley and time of John Kaminsky at the Max Planck Institute for Dynamics and Self-Organization. We are grateful to Eberhard Bodenschatz for fruitful discussions and the possibility to utilize the data.

References

- Anderson Jr., J.D.: A History of Aerodynamics: and Its Impact on Flying Machines, vol. 8. Cambridge University Press, Cambridge (1999)
- Baals, D.D., Corliss, W.R.: Wind Tunnels of NASA, vol. 440. National Aeronautics and Space Administration, Scientific and Technical Information Branch, Washington, D.C. (1981)
- Barndorff-Nielsen, O.E.: Exponentially decreasing distributions for the logarithm of the particle size. *Proc. R. Soc. Lond. A* **353**, 401–419 (1977)
- Bernard, P.S., Wallace, J.M.: Turbulent Flow. Wiley, Hoboken (2002)
- Bhattacharya, R., Waymire, E.C.: Stochastic Processes with Application. Wiley, New York (1990)
- Birnik, B.: The Kolmogorov–Obukhov statistical theory of turbulence. *J. Nonlinear Sci.* **23**, 657–688 (2013a). <https://doi.org/10.1007/s00332-012-9164-z>
- Birnik, B.: The Kolmogorov–Obukhov Theory of Turbulence. Springer, New York (2013b)
- Birnik, B.: From Wind-Blown Sand to Turbulence and Back, pp. 15–27. Springer, Cham (2016)
- Blum, D.B., Bewley, G.P., Bodenschatz, E., Gibert, M., Gylfason, A., Mydlarski, L., Voth, G.A., Xu, H., Yeung, P.K.: Signatures of non-universal large scales in conditional structure functions from various turbulent flows. *New J. Phys.* **13**, 113020 (2011)
- Bodenschatz, E., Bewley, G.P., Nobach, H., Sinhuber, M., Xu, H.: Variable density turbulence tunnel facility. *Rev. Sci. Instrum.* **85**(9), 093908 (2014)
- Comte-Bellot, G., Corrsin, S.: The use of a contraction to improve the isotropy of grid-generated turbulence. *J. Fluid Mech.* **25**(04), 657–682 (1966)
- Corrsin, S.: Turbulent flow. *Am. Sci.* **49**(3), 300–325 (1961)
- Da Prato, G., Zabczyk, J.: Encyclopedia of Mathematics and Its Applications: Stochastic Equations in Infinite Dimensions. Cambridge University Press, Cambridge (2014)
- Dubrulle, B.: Intermittency in fully developed turbulence: in log-Poisson statistics and generalized scale covariance. *Phys. Rev. Lett.* **73**(7), 959–962 (1994)
- Grimmett, G., Stirzaker, D.: Probability and Random Processes. Oxford University Press, Oxford (2001)
- Hunt, B.R., Sauer, T., Yorke, J.A.: Prevalence: a translation-invariant almost every on infinite-dimensional spaces. *Bull. Am. Math. Soc.* **27**(2), 217–238 (1992)
- Kolmogorov, A.N.: Dissipation of energy under locally isotropic turbulence. *Dokl. Akad. Nauk SSSR* **32**, 16–18 (1941a)
- Kolmogorov, A.N.: The local structure of turbulence in incompressible viscous fluid for very large Reynolds number. *Dokl. Akad. Nauk SSSR* **30**, 9–13 (1941b)
- Kolmogorov, A.N.: A refinement of previous hypotheses concerning the local structure of turbulence in a viscous incompressible fluid at high Reynolds number. *J. Fluid Mech.* **13**, 82–85 (1962)
- Landau, L.D., Lifshits, E.M.: Fluid Mechanics: Transl. from the Russian by JB Sykes and WH Reid. Addison-Wesley, New York (1959)
- Millikan, C.B., Smith, J.E., Bell, R.W.: High-speed testing in the Southern California cooperative wind tunnel. *J. Aeronaut. Sci.* **15**(2), 69–88 (1948)
- Oksendal, B.: Stochastic Differential Equations. Springer, New York (1998)
- Pope, S.B.: Turbulent Flows. Cambridge University Press, Cambridge (2000)
- Prandtl, L.: Göttingen wind tunnel for testing aircraft models. National Advisory Committee for Aeronautics, Washington, DC (1920)

- Reynolds, O.: On the dynamical theory of incompressible viscous fluids and the determination of the criterion. *Philos. Trans. R. Soc. Lond.* **186A**, 123–164 (1885)
- She, Z.-S., Leveque, E.: Universal scaling laws in fully developed turbulence. *Phys. Rev. Lett.* **72**(3), 336–339 (1994)
- She, Z.-S., Waymire, E.: Quantized energy cascade and log-Poisson statistics in fully developed turbulence. *Phys. Rev. Lett.* **74**(2), 262–265 (1995)
- Sinhuber, M., Bewley, G.P., Bodenschatz, E.: Dissipative effects on inertial-range statistics at high Reynolds numbers. *Phys. Rev. Lett.* **119**, 134502 (2017)
- Sinhuber, M., Bodenschatz, E., Bewley, G.P.: Decay of turbulence at high Reynolds numbers. *Phys. Rev. Lett.* **114**, 034501 (2015)
- Taylor, G.I.: Statistical theory of turbulence. *Proc. R. Soc. Lond.* **151**, 421–444 (1935)
- Vallikivi, M., Smits, A.J.: Fabrication and characterization of a novel nanoscale thermal anemometry probe. *J. Microelectromech. Syst.* **23**(4), 899–907 (2014)
- Walsh, J.B.: An introduction to stochastic differential equations. In: Dold, A., Eckmann, B. (eds.) *Springer Lecture Notes*. Springer, New York (1984)

Publisher's Note Springer Nature remains neutral with regard to jurisdictional claims in published maps and institutional affiliations.

Affiliations

John Kaminsky¹  · Björn Birnir^{1,3} · Gregory P. Bewley² · Michael Sinhuber⁴

✉ John Kaminsky
jkaminsky@math.ucsb.edu

¹ CNLS and Department of Mathematics, UC Santa Barbara, Santa Barbara, USA

² Department of Mechanical Engineering, Cornell University, Ithaca, USA

³ CNLS and Department of Mathematics, University of Iceland, Reykjavík, Iceland

⁴ Department of Civil and Environmental Engineering, Stanford University, Stanford, USA